Czech Technical University in Prague

Faculty of Electrical Engineering

Department of Microelectronics

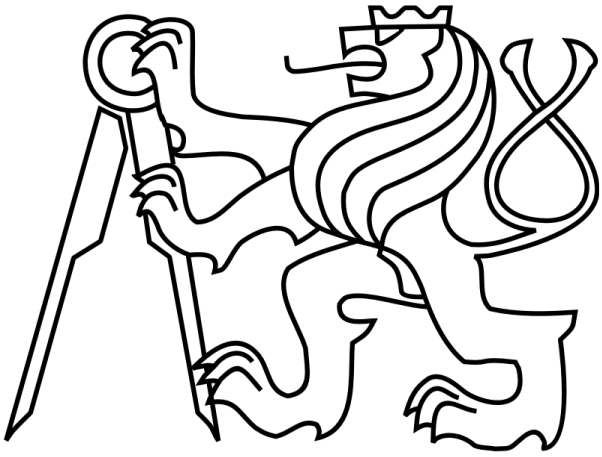

Bachelor thesis

Carbon nanostructure research

Author: Bogdan Miasoiedov

Supervisor: doc. RNDr. Jan Voves CSc.

2017

ČESKÉ VYSOKÉ UČENÍ TECHNICKÉ V PRAZE

ZADÁNÍ BAKALÁŘSKÉ PRÁCE

I. OSOBNÍ A STUDIJNÍ ÚDAJE

Příjmení: **Miasoiedov** Jméno: **Bogdan** Osobní číslo: **439644**

Fakulta/ústav: **Fakulta elektrotechnická**

Zadávající katedra/ústav: **Katedra mikroelektroniky**

Studijní program: **Komunikace, multimédia a elektronika**

Studijní obor: **Komunikace a elektronika**

II. ÚDAJE K BAKALÁŘSKÉ PRÁCI

Název bakalářské práce:

Výzkum uhlíkových nanostruktur

Název bakalářské práce anglicky:

Carbon Nanostructure Research

Pokyny pro vypracování:

1. Prostudujte problematiku přípravy grafénu na karbidu křemíku.
2. Posuďte realizovatelnost vybraných metod přípravy grafénu na katedře mikroelektroniky ČVUT FEL.
3. Experimentálně ověřte realizovatelnost vybraných metod.

Seznam doporučené literatury:

[1] Riedl, C., Epitaxial graphene on silicon carbide surfaces: growth, characterization, doping and hydrogen intercalation, 2010
[2] Mikhailov, S., Physics and applications of graphene - experiments, Croatia: InTech, ISBN: 978-953-307-217- 3, 2011

Jméno a pracoviště vedoucí(ho) bakalářské práce:

doc. RNDr. Jan Voves CSc., katedra mikroelektroniky FEL

Jméno a pracoviště druhé(ho) vedoucí(ho) nebo konzultanta(ky) bakalářské práce:

Datum zadání bakalářské práce: **17.02.2017** Termín odevzdání bakalářské práce: _____

Platnost zadání bakalářské práce: **10.08.2018**

Podpis vedoucí(ho) práce	Podpis vedoucí(ho) ústavu/katedry	Podpis děkana(ky)

III. PŘEVZETÍ ZADÁNÍ

Student bere na vědomí, že je povinen vypracovat bakalářskou práci samostatně, bez cizí pomoci, s výjimkou poskytnutých konzultací. Seznam použité literatury, jiných pramenů a jmen konzultantů je třeba uvést v bakalářské práci.

21.6.2017
Datum převzetí zadání

Podpis studenta

HONEST DECLARATION

I hereby declare that this bachelor thesis is completely my own work and that I used only the cited sources in accordance with the Methodical instruction about observance of ethical principles of preparation of university final projects.

Prague, July 31, 2017

. . . . . .

Signature

ABSTRACT

Successful experiments conducted by Manchester's group in 2004 have attracted a great number of researches of studying graphene. It possesses certain remarkable properties that are briefly discussed in the thesis. Main focus has been aimed to the methods of graphene growth, as long as usage of this material in industry still remains a big issue.

Among different techniques of graphene production, closer attention has been paid to epitaxial graphene growth by silicon carbide (SiC) sublimation. Various articles concerning the method have been studied and the conditions used in the experiments, conducted by different research groups, have been summarized in tables. This investigation allowed to compare available research possibilities and to choose the most appropriate methodology in order to try graphene production by SiC sublimation at the department of microelectronics. Unfortunately, such the experiment has become impossible during the work on the thesis due to technical reasons. Therefore, in addition graphene nanoribbons (GNRs) chemical synthesis from precursors has been considered.

ANOTACE

Úspěšné experimenty provedené skupinou z univerzity v Manchesteru v roce 2004 stimulovaly velké množství výzkumných prací zabývajících se grafénem. Tento material má pozoruhodné vlastnosti, které jsou v práci stručně probírány. Hlavní pozornost je zaměřena na metody růstu grafénu, jelikož využití tohoto materiálu v průmyslu stále zůstává velkým problémem.

Mezi rozdílné metod přípravy grafenu je pozornost soustředěna na epitaxní růst grafénu sublimací karbidu křemičitého (SiC). Byly studovány publikace zabývající se touto metodou. Podmínky užité při experimentech provedených různými výzkumnými skupinami byly shrnuty v tabulkách. Byly porovnány použité metody a jejich parametry. Byla vybrána nejvhodnější metodologie při pokusu o výrobu grafenu sublimací SiC na katedře mikroelektroniky. Tento experiment bohužel nebylo možné dokončit z technických důvodů. Navíc byla proto také zkoumána syntéza grafénových nanoribonů (GNRs) z prekurzorů.

CONTENTS

LIST OF FIGURES

LIST OF TABLES

LIST OF ACRONYMS

CMOS Complementary metal-oxide semiconductor

AFM Atomic force microscopy

CVD Chemical vapor deposition

UHV Ultrahigh vacuum

STM Scanning tunneling microscopy

LEEM Low-energy electron microscopy

GNR Graphene nanoribbon

ML Monolayers

1 INTRODUCTION

Modern electronics is presently facing numerous challenges concerning maintenance of current tempo of development. This problem regarding the most common CMOS (complementary metal-oxide-semiconductor) technology is discussed in [1], rather globally and exhaustively. According to [1], the challenges can be split in the following categories:

1. **Physical** (increment of tunneling and leakage currents as the devices are becoming smaller, thus impacts the performance and functionality of CMOS devices).
2. **Material** (inability of the dielectric and wiring materials to provide reliable insulation and conduction, respectively with continued scaling).
3. **Power-thermal** (increasing number of transistors integrated per unit-area, which demands larger power consumption and higher thermal dissipation).
4. **Technological** (incompetency of lithography-based techniques to provide the resolution below the wavelength of the light to manufacture CMOS devices).
5. **Economical** (rising in cost of production, fab, and testing that may reach a point where it will be not affordable from economic point of view).

Those points lead to a conclusion that we should find new technologies and materials, which will enable us to utilize fundamentally different principles. However, the innovation has to involve rather big margin of currently available technological processes and materials in order to maintain reasonable production costs.

As to look at the material perspective, the most common subject of present research in the field is graphene, the material which possess certain remarkable properties, yet suffers from the technological point of view, because most of current technologies concerning the production of devices based on graphene cannot compete with the CMOS. However, quite plausible solution to the issue can be the epitaxial graphene growth on silicon carbide (SiC), which will be discussed further in the work together with graphene.

The goal of this project is to study some of graphene properties, problematics of the graphene growth methods on SiC and to consider the application of one of the methods, taking into account available possibilities.

2 GRAPHENE

Graphene is the name given to a single layer of carbon atoms densely packed into a benzene-ring structure (Figure 1). It is widely used to describe properties of many carbon-based materials, including graphite, large fullerenes, nanotubes, etc. (e.g., carbon nanotubes are usually thought of as graphene sheets rolled up into nanometer-sized cylinders). Also graphene has been reported to be an aromatic molecule [2]. Planar graphene itself has been presumed not to exist in the free state, being unstable with respect to the formation of curved structures such as soot, fullerenes, and nanotubes. [3]

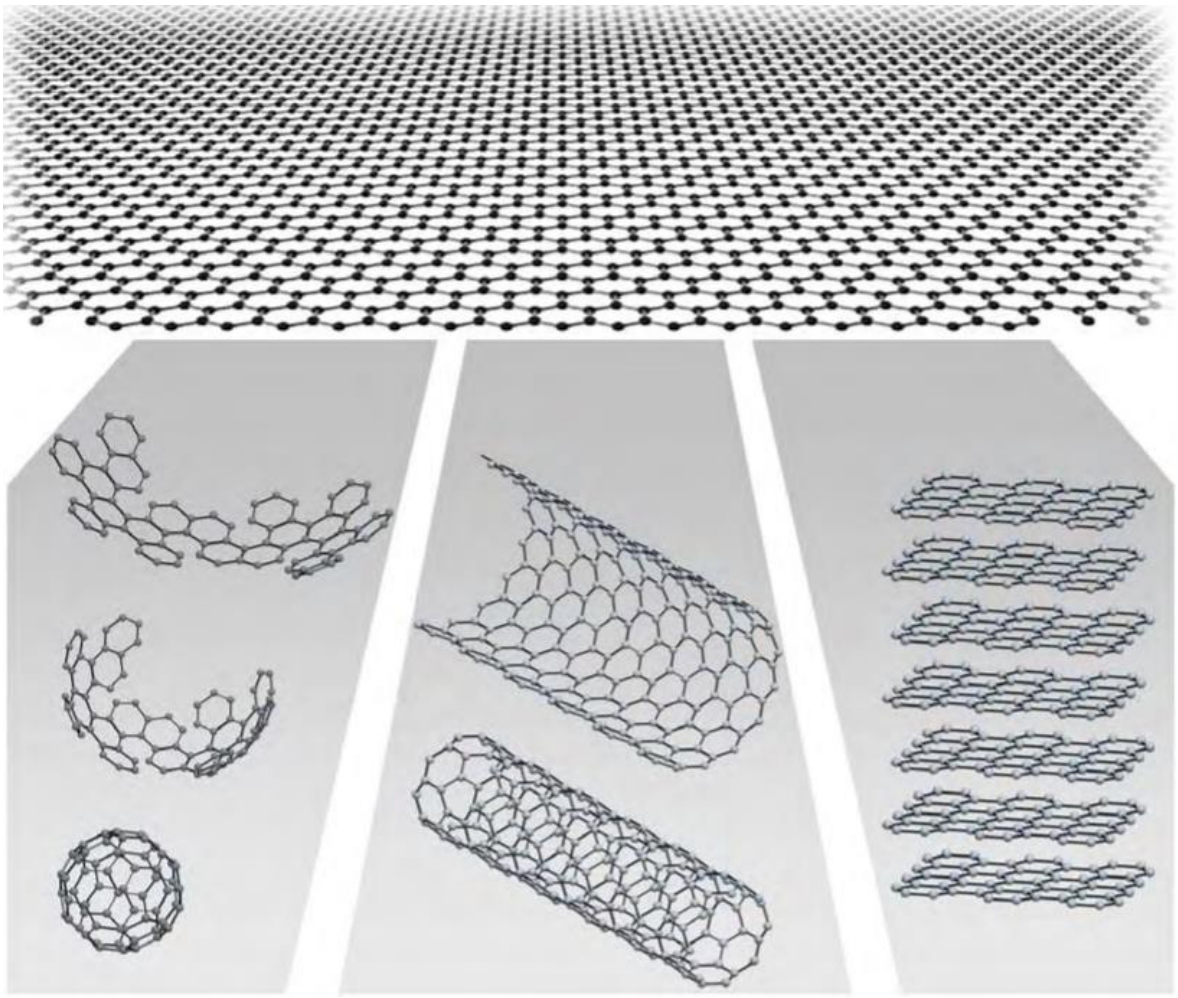

Figure 1. Graphene, mother of all graphitic forms. The image is taken from Ref. [4].

Graphene had already been studied theoretically in 1947 by P.R. Wallace as a text book example for calculations in solid state physics [5]. He predicted the electronic structure and noted the linear dispersion relation. The wave equation for excitations was written down by J.W. McClure already in 1956, and the similarity to the Dirac equation was discussed by G.W. Semenoff in 1984.

It came as a surprise to the physics community when Andre Geim, Konstantin Novoselov and their collaborators from the University of Manchester (UK), and the Institute for Microelectronics Technology in Chernogolovka (Russia), published their results on graphene structures in October of 2004 in Science [3]. They described the fabrication,

identification and Atomic Force Microscopy (AFM) characterization of graphene. The method used for the fabrication was first suggested and tried by R. Ruoff's group. It implies simple but effective procedure of extracting thin layers of graphene by means of mechanical exfoliation using sticky Scotch tape and transferring those layers onto silicon substrate. However, R. Ruoff's group did not succeed in identification of any monolayers. On the other hand Manchester group used an optical method which enabled them to identify fragments made up of only few layers of graphene. An AFM picture of one such sample is shown in the Figure *2*. In some cases these flakes were made up of a single layer, i.e. planar graphene was identified. [6]

Figure 2. Atomic Force Microscopy (AFM) picture of a monolayer of graphene. The black area is the substrate, the dark orange is a mono layer of graphene and has a thickness of ~0.5nm, the bright orange part contains a few layers and has a thickness of ~2nm. The image is taken from Ref. [6].

In 2010 Andre Geim and Konstantin Novoselov were awarded the Nobel Prize in physics "for groundbreaking experiments regarding the two-dimensional material graphene" [6].

2.1 Electronic structure of monolayer graphene

Besides being the first discovered one-atom-thick material, graphene offers amazing prospects both for fundamental physics and technology. Its peculiar electronic properties are caused by simple but unique lattice, which is formed by hexagonal planar structure thanks to the sp^2-hybridization between one *s* orbital and the p_x-, p_y-orbitals (Figure 3). The *σ*-bonds are formed by the in-plane sp^2-orbitals as sketched in the Figure 3. These bonds are responsible for the robustness of graphene's structure. As the *σ*-bands have a filled shell due to the Pauli principle, they form a deep valence band far away from the Fermi level. The

unaffected p_z-orbital is oriented perpendicular to the planar structure and forms covalent π-bonds with the neighbouring carbon atoms. These bonds result in the π-band, which is half filled and is responsible for the conductivity.

Graphene's hexagonal lattice is displayed in the Figure 4a. It exhibits a basis of two atoms per unit cell. As a consequence, graphene consists of two equivalent sublattices marked A (green) and B (red). The lattice vectors of graphene can be written in the following way:

$$\vec{a}_1 = \frac{a}{2}(\sqrt{3}, -3), \qquad \vec{a}_2 = \frac{a}{2}(\sqrt{3}, 3),$$

with $a \approx 1.42$ Å being the C-C bond length. The corresponding reciprocal lattice of graphene and its Brillouin zone is shown in the Figure 4b. The reciprocal lattice vectors are

$$\vec{b}_1 = \frac{2\pi}{3a}(\sqrt{3}, -1), \qquad \vec{b}_2 = \frac{2\pi}{3a}(\sqrt{3}, 1).$$

The corners of the Brillouin zone are of particular importance for the physics of graphene. They are $\overline{K}$- and $\overline{K'}$-point respectively (Figure 4b) and are often designated as different "valleys", due to the two graphene sublattices.

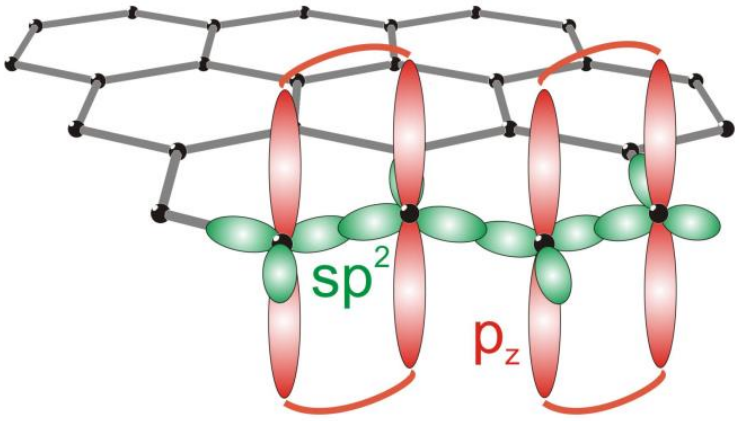

Figure 3. Graphene lattice structure with its sp^2-hybridized carbon atoms. The image is taken from Ref. [7].

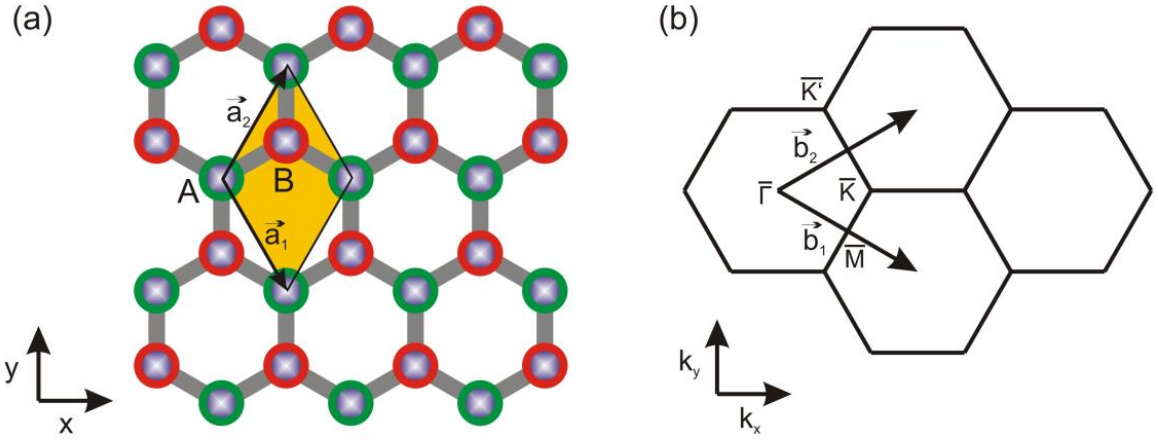

Figure 4. (a) Honeycomb lattice structure of graphene with a unit cell comprising a basis of two atoms, which leads to two equivalent sublattices. The nature of the crystal structure stands behind all the

spectacular properties of graphene. (b) Graphene Brillouin zone in reciprocal space together with the reciprocal unit vectors. The image is taken from Ref. [7].

The electronic band structure can be quite easily determined from an analytical tight binding approach. The first tight binding description was given by P.R. Wallace. He considered nearest- and next-nearest-neighbor interaction for the graphene p_z-orbitals, but neglected the overlap between wave functions centered at different atoms. Probably better known nowadays, tight binding approximation by Saito et al. includes this overlap integral, but considers only interactions between nearest neighbors within the graphene sheet. The dispersion relation *E*(*k*) of the *π*-bands as calculated from the original description [5] is given by:

$$E_{\pm}(\vec{k}) = \pm t\sqrt{3 + f(\vec{k})} - t' f(\vec{k}),$$

$$\text{with} \quad f(\vec{k}) = 2cos(\sqrt{3}k_y a) + 4\cos\left(\frac{\sqrt{3}}{2}k_y a\right) cos\left(\frac{3}{2}k_x a\right),$$

where the plus sign belongs to the upper conduction (*π**-) and the minus sign to the lower valence (*π*-) band, the parameter *t* is the nearest-neighbor hopping energy (hopping between different sublattices) and *t'* is the next nearest-neighbor hopping energy (hopping in the same sublattice). The corresponding band structure is plotted in the Figure 5a with *t* = 2.7 eV and *t'* = 0.2 *t* . If the next nearest-neighbor interaction is neglected, the valence and the conduction bands become symmetric, a representation, which is also quite often used in visualizations of graphene's band structure. A non-zero overlap integral similarly breaks the symmetry between the *π*- and *π∗*-bands. Both approaches by Wallace and Saito et al. give a quite good approach for the energy dispersion of the *π*-bands. For a more accurate description, in particular away from the high symmetry directions, ab initio calculations are necessary or interactions up to the third nearest neighbor have to be included in the tight binding descriptions. To have a complete overview of graphene's valence band structure, Figure 5b shows both the *π*- and *σ*-bands of graphene as determined from the tight binding description by Saito et al.. As mentioned earlier the three *σ*-bands are far below the Fermi level E_F ($E_F = 0$). The *π*- and *π**-bands however meet each other at the Fermi energy at the $\overline{K}$- and $\overline{K'}$-points. This crossing point is called Dirac point (E_D). As the involved electrons belong to two different sublattices, an energy gap is not opened. Consequently, graphene can be seen as a zero-gap semiconductor or as a zero-overlap semimetal. As highlighted by the zoom in the Figure 5a, the *π*-bands exhibit another peculiarity, namely a linear dispersion around the Dirac point. A first order expansion around the $\overline{K}$- (or $\overline{K'}$-) point of $E(\vec{K} + \vec{q})$ with $|\vec{q}| \ll |\vec{K}|$ yields

$$E_{\pm}(\vec{q}) \approx \pm\hbar v_F |\vec{q}|,$$

where $v_F = 3ta/2\hbar$ is the so-called Fermi velocity and the vector $\vec{K}$ denotes the position of the $\overline{K}$-point in momentum space with its origin located at $\overline{\Gamma}$. The Fermi velocity amounts to $1 \cdot 10^6\, m/s$. For condensed matter systems the parabolic dispersion $\hbar^2 q^2/(2m)$ would usually be expected, where *m* is the electron mass. The velocity in such a case depends on the energy: $v = \sqrt{2E/m}$. It should be noted that a second order expansion of $E(\vec{K} + \vec{q})$ results in a direction dependence in momentum space. Constant energy maps show a threefold symmetry, which is called trigonal warping. [7]

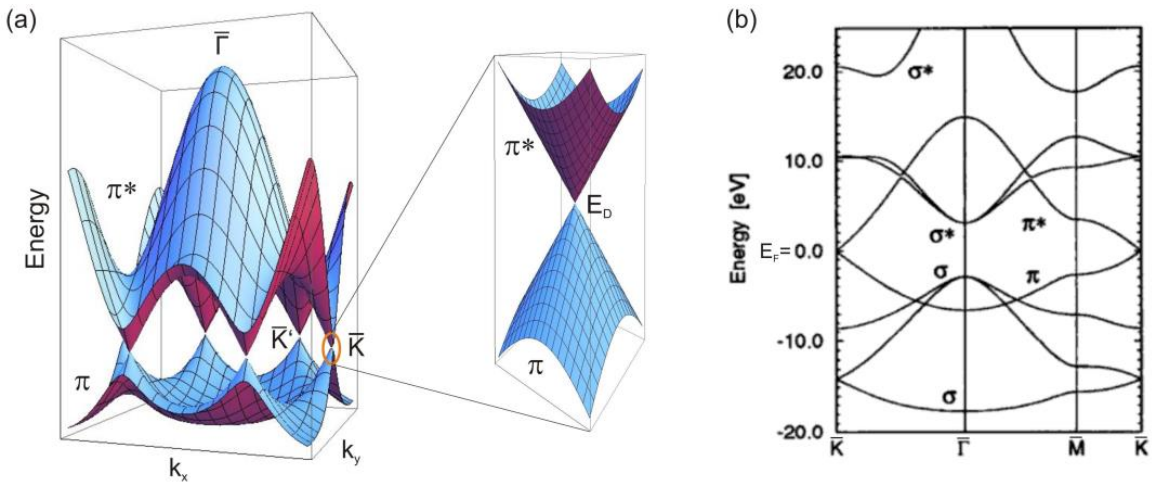

Figure 5. (a) The graphene π-band dispersion in three-dimensional representation as calculated from the original tight-binding approach by P.R. Wallace. The nearest and next nearest-neighbor interaction parameters are set to t = 2.7 eV and t' = 0.2t, respectively. The inset shows a zoomed region close to the $\bar{K}$-point where a linear band structure can be observed. (b) The π- and σ-bands of graphene as calculated from the tight-binding approach by Saito et al.. The image is taken from Ref. [7].

3 METHODS OF GRAPHENE PREPARATION

Techniques developed for synthesizing graphene can be grouped into six major categories, i.e., mechanical cleavage, epitaxial growth by SiC sublimation, chemical vapor deposition (CVD), total organic synthesis, and chemical method. The first attempt to produce graphene goes back to 1960, when the electron microscopist, Fernandez-Moran, was looking for a robust, electron-beam transparent, and uniform support membrane. Millimeter-sized graphene sheets as thin as 5 nm (~ 15 layers of graphene) were produced by micromechanical exfoliation from graphite. Single layers and bilayers of colloidal graphite oxide were observed by electron microscopy by Boehm et al. in 1962. Chemical intercalation and exfoliation of oxidized graphite were extensively investigated in the next decade. Since the discovery of fullerenes and nanotubes in the early 1990s, great interests were attracted to study all kinds of carbon materials including graphene. Nanoscale origami-like structures of one layer graphene thickness were observed by atomic force microscopy (AFM) manipulation of freshly cleaved pyrolytic graphite. Sub-10 nm stacks of graphite were obtained by rubbing micro fabricated graphite pillars on a substrate in 1999, suggesting a possibility to produce single layer using this technique. As it was mentioned before, Geim's group successfully extracted monolayer graphene sheets by repeatedly cleaving a graphite crystal with an adhesive tape to its limit in 2004. The success in mechanical cleavage led to the synthesis of graphene using other techniques that had reputedly failed in the past. Among others, epitaxial growth by SiC sublimaiton and CVD were shown to produce high-quality graphene. New methods have emerged to transfer CVD-grown graphene to other substrates for applications in devices. In order to produce large quantities of graphene for industry applications, developing large-scale and mass production methods became necessary. Among those feasible for large-scale production include the total organic synthesis of polyaromatic hydrocarbons (PAH) and the chemical route to produce reduced graphene oxide (rGO) sheets. At present, the chemical method has emerged to be a viable route to afford graphene-based single sheets in considerable quantities.

Method	Advantages	Disadvantages
Mechanical cleavage	Less defects	Neither scalable nor capable for mass production
Epitaxial growth by SiC sublimation	No defects for every single graphene island	Discontinuous
Chemical vapor deposition (CVD)	Compatible with the current CMOS technologies	High cost and complex transfer process
Total organic synthesis	Potentially suitable for mass production	Many defects
Chemical method	Low cost and suitable for mass production	The majority of defects can be removed

Table 1. Brief summary of graphene growth methods. The table is taken from Ref. [8].

The Table 1 summarizes the relative advantages and disadvantages of the above mentioned synthesis methods in term of the feasibility to scale-up the process for mass production, materials and production costs, and the presence of defects. [8]

3.1 CVD growth on metal surfaces

Integrated devices will require wafer scale deposition that can be processed using existing complementary metal oxide semiconductor (CMOS) fabrication techniques. Implementation as a transparent conductor will demand uniform deposition over large areas with controllable number of graphene layers. These requirements have led to the development of a rapidly evolving research thrust within the field of graphene based on deposition of high quality and uniform thin films over large areas with controllable thickness.

The most promising, inexpensive and readily accessible approach for deposition of reasonably high quality graphene is chemical vapor deposition (CVD) onto transition metal substrates such as Ni, Pd, Ru, Ir or Cu. In particular, recent developments on uniform single layer deposition of graphene on copper foils over large areas have allowed access to high quality material. Although CVD of graphene on copper is relatively new, several groups around the world have already reported excellent device characteristics such as mobilities of up to 7350 $cm^2V^{-1}s^{-1}$ at low temperature and large area growth (up to 30 inches). [9]

Chemical vapor deposition is a widely used material-processing technology. The majority of its applications involve applying solid thin-film coatings to surfaces, but it is also used to produce high-purity bulk materials and powders, as well as fabricating composite materials via infiltration techniques.

CVD involves flowing a precursor gas or gases into chamber containing one or more heated objects to be coated. Chemical reactions occur on and near the hot surfaces, resulting in the deposition of a thin film on the surface. This is accompanied by the production of chemical by-products that are exhausted out of the chamber along with unreacted precursor gases. As would be expected with the large variety of materials deposited and the wide range of applications, there are many variants of CVD. It is done in hot-wall reactors and cold-wall reactors, at sub-torr total pressures to above-atmospheric pressures, with and without carrier gases, and at temperatures typically ranging from 200 to 1600ºC. [10]

3.1.1 Graphene CVD

In CVD of graphene, a metal substrate such as copper is put into a furnace and heated under low vacuum to around 1000°C. The heat anneals the copper, increasing its domain size. Methane and hydrogen gases are then flowed through the furnace. The hydrogen catalyzes a reaction between methane and the surface of the metal substrate, causing carbon atoms from the methane to be deposited onto the surface of the metal through chemical adsorption (Figure 6). The furnace is quickly cooled to keep the deposited carbon layer from aggregating into bulk graphite, which crystallizes into a contiguous graphene layer on the surface of the metal. [11]

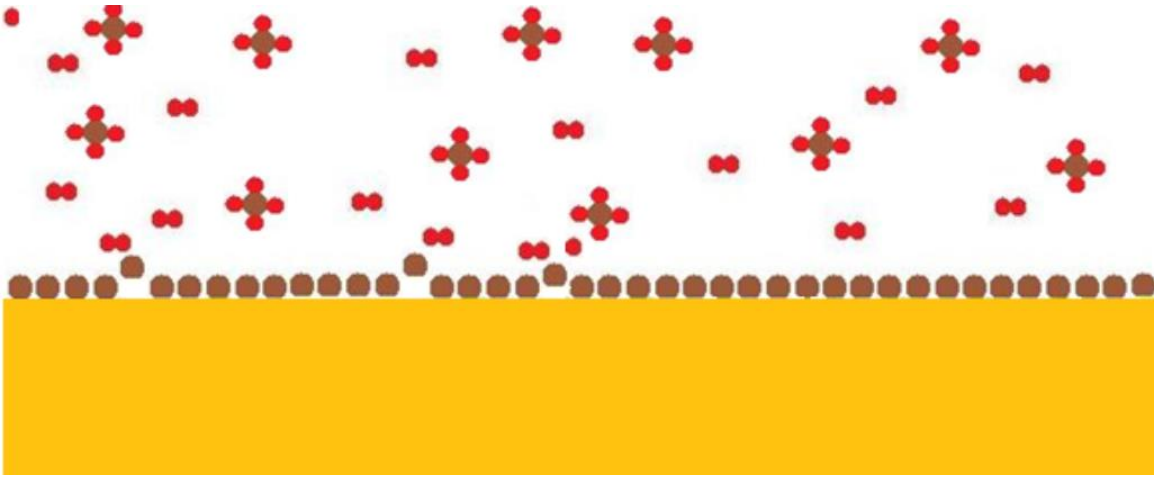

Figure 6. Diagram of CVD growth on copper. The image is taken from Ref. [11].

The graphene produced by this method is more likely to carry impurities due to the various materials required for CVD. However, research has shown that such impurities can be sufficiently minimized to create graphene as pure as exfoliated flakes. Additionally, the graphene from CVD tends to wrinkle due to the difference in thermal expansion between graphene and copper. This is decreased via proper annealing, but is still an ongoing research challenge. Most importantly, graphene from CVD is a contiguous film as large as the underlying metal substrate, in stark contrast to the random micron-sized flakes from the scotch tape method. CVD thus allows graphene to be used in a solar cell. [11]

There are many ways to affect the outcome of a CVD graphene growth run. Since the growth dynamics of carbon deposition and domain growth are not yet fully understood, finding the proper balance of these controls is a largely experimental task. Perhaps the most natural variable to affect a CVD outcome is the amount of the various reaction gases. Increased methane provides more carbon atoms to deposit (and more nucleation sites leading to more domains), while increased hydrogen promotes the reaction and also increases chemical processes on the copper and surrounding environment. The temperature also affects the rate of reaction, as does the speed of changes in temperature. Impurities in the copper substrate detract from the growth process by encouraging nucleation sites and thus hindering the formation of contiguous carbon domains, so proper chemical cleaning of the copper is essential. Annealing time of the copper also affects the level of impurity for the same reason. The geometry of the growth chamber affects the deposition rate of carbon due to its effect on gas flow patterns, specifically because of turbulent (instead of laminar) flow regimes. Finally, any leaks in the vacuum system further detract from the growth, as oxygen from the air oxidizes the copper, making the carbon atoms unable to adhere to the copper surface and ruining the deposition. [11]

It should be noted that graphene CVD on nickel is somewhat common, and cobalt has also been used. The main differences between metal substrates come from differences in the metals' ability to absorb carbon. Nickel and cobalt absorb carbon more than copper, and this leads to an overabundance of carbon on foils which crystallizes into discrete graphite chuncks instead of a single graphene sheet. For that reason, nickel and cobalt foils cannot be used and instead thin films (< 300nm for nickel) must be evaporated onto a silicon substrate before growth. Copper, on the other hand, attracts less carbon and does so only at the surface rather than absorbing it into the bulk of the material, since the weak bonds

that hold the carbon atoms to the copper can only be formed with open bonding sites at the surface of the lattice. Therefore, copper foils can be used in graphene CVD, simplifying the production process as a whole and making it more robust. [11]

A fairly common variant on CVD is that of plasma-enhanced CVD. PECVD works in much the same way as has already been described, but in addition to using a furnace to provide the heat energy for substrate annealing, an RF frequency AC current is passed through the substrate. This spark ionizes the gases in the chamber, enhancing the deposition onto the substrate. PECVD can be done at much lower furnace temperatures than regular CVD. [11]

3.1.2 Transfer process

Another key advantage to CVD graphene growth is the ability to transfer the graphene to an arbitrary substrate (Figure 7). Once the graphene/copper foil has been removed from the furnace and cooled, a polymer such as polydimethylsiloxane (PDMS) or polymethylmethacrylate (PMMA) can be spin coated onto the graphene as a support, and then the copper removed using an etchant such as ferric chloride ($FeCl_3$). This leaves the graphene attached only to the polymer, which can be positioned onto any other substrate (such as a solar cell). A solvent can easily dissolve the polymer, leaving just the graphene on any desired substrate. [11]

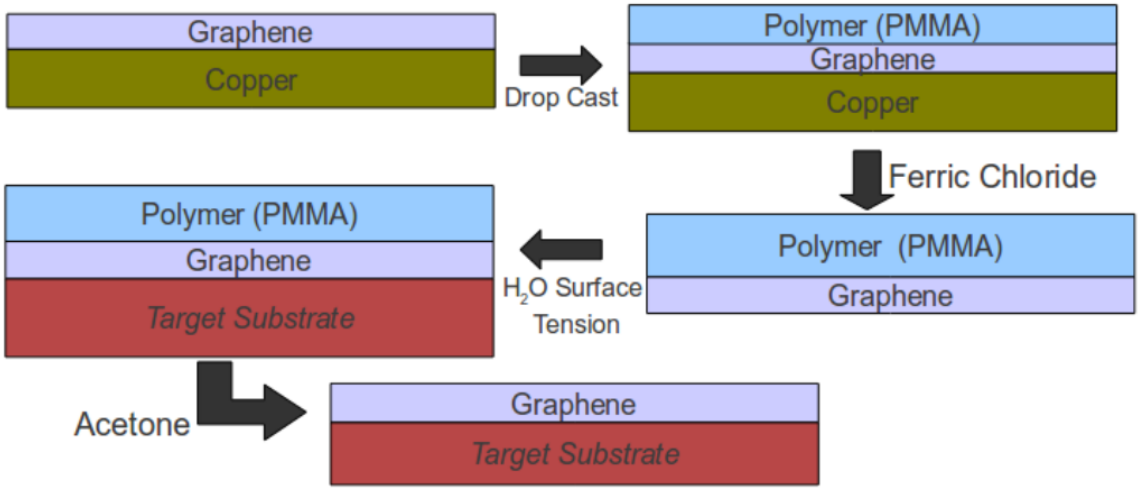

Figure 7. Schematic diagram of the transfer process to an arbitrary substrate. The image is taken from the Ref. [11].

3.2 Epitaxial graphene by SiC sublimation

Transfer-free wafer-scale graphene growth is possible by the thermal decomposition of silicon carbide (SiC). The fundamental phenomenon is illustrated in the Figure 17. When we heat the SiC in a vacuum or in an argon atmosphere, only the silicon atoms leave the surface due to the difference in the vapor pressures of silicon and carbon, and the remaining carbon atoms form epitaxial graphene spontaneously on the surface. One of the advantages of this technique is that commercially available semi-insulating SiC wafers can be used. [12]

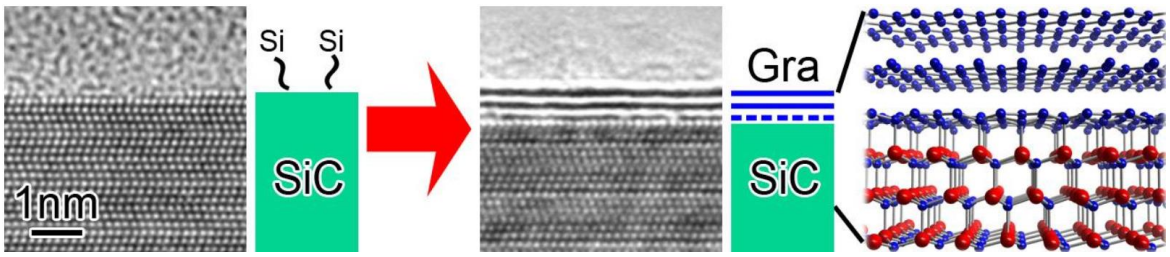

Figure 8. Basics of graphene growth by thermal decomposition of SiC, together with the structural model of bilayer graphene on SiC. Shown as the blue broken line in the buffer layer. The image is taken from Ref. [12].

It is believed (although not yet fully established) that as the growth progresses graphene layers are formed between current graphene layers and the SiC surface, i.e. secondary layers grow underneath the primary one. [13]

While the initial studies involving growth under UHV required heating to about 1600 K for control of the thickness of the graphene film, now samples of better controlled quality are grown under rougher conditions, but require higher heating temperatures. Under a Si-rich atmosphere or by using a buffer gas, high quality samples are indeed prepared at temperatures of about 1900 K. [13]

Graphene formation is dependent on the structure of the SiC surface. The most commonly used SiC polytype structures for growing epitaxial graphene are 4H-SiC and 6H-SiC. Both of these lattices have either a Si- or C-terminated surface. These are the (0001) surface for Si termination and the $(000\bar{1})$ surface for C termination. The growth of the graphene and its final structure are dependent on which of these surfaces is initially exposed. On the Si-terminated surface the graphene layer produced has an orientation of 30° with respect to the SiC plane. For the C-surface the growth is faster but the graphene has a variety of different orientations. Because of this most studies of graphene growth on SiC have focused on the Si-terminated surface. [13]

Pre-patterned SiC surfaces, for instance, with arrays of trenches with abrupt walls created by lithography, were found to spontaneously transform into inclined facets with a well-defined surface normal other than (0001) or $(000\bar{1})$ under annealing. Graphene growth on such patterned surfaces was found to be preferential on the inclined facets, so that extended graphene ribbons, with size determined by the depth of the initial trenches, can be obtained in a rather versatile manner. [13]

3.2.1 The growth process

To produce graphene using Si sublimation, the SiC surface must first be treated. Scratches are removed by etching with hydrogen, and then the SiC is rapidly heated to the growth temperature, typically between 1473 and 1933 K, for a specific time. During the heating process a Si flux is applied to remove any produced SiO gas and maintain the concentration of Si on the surface. Alternatively, growth can be performed under an Ar atmosphere. The SiC is then cooled at a slower rate until reaching room temperature. The etching process forms regular steps along the surface of the SiC, which are a unit cell in height. [13]

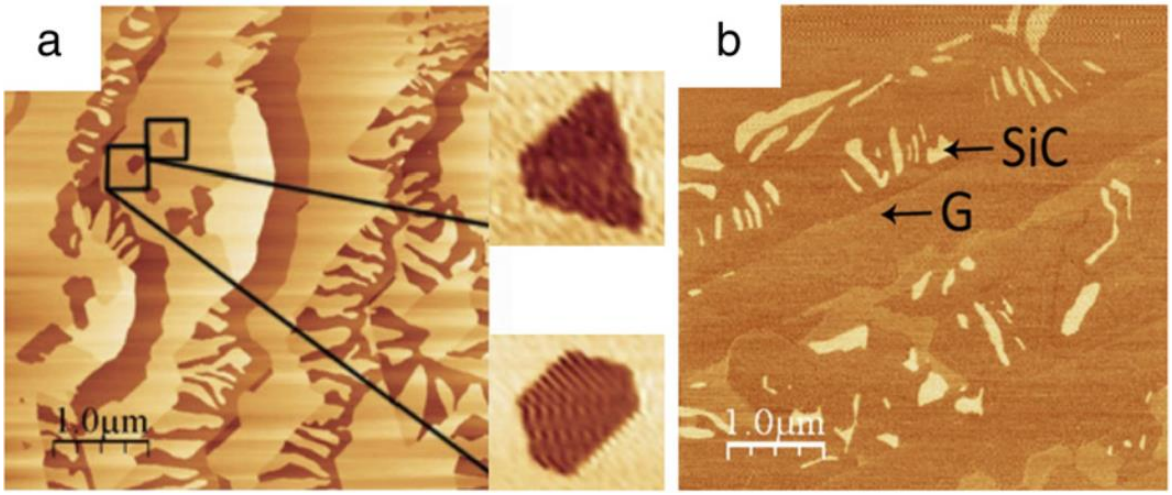

Figure 9. AFM topography of the SiC surface after heating to (a) 1748 K and (b) 1823 K. At 1673 K no graphene is present (shown using AFM phase measurements). At 1748 K fingers are formed with graphene in between them (a) (two terrace pits highlighted in the AFM image are shown separately at high resolution) and these eventually erode to become islands (b). At 1873 K the islands have completely eroded and graphene covers the whole surface. The image is taken from Ref. [13].

According to [13], to understand how graphene grows from this process, the 4H-SiC (0001) surface was monitored as the growth temperature and heating time were separately varied. In each case AFM (tapping mode) and STM were used to observe the changes on the surface and the progression of graphene growth. Scans were performed in a nitrogen environment at atmospheric pressure. To determine the temperature dependence of the growth the SiC was heated to a range of different temperatures between 1673 and 1873 K for 10 min. At 1673 K no graphene was found on the surface, however pits in the SiC surface had started to develop on the terraces. Increasing the temperature increased the fraction of the surface covered by pits. At 1748 K, see Figure 9a, the bottom of a pit was analyzed with high STM magnification. Taking a 2D Fast Fourier transform of the STM data revealed the hexagonal structure of graphene. From this it was assumed that there are two phases present on the surface: reconstructed SiC on the surface terrace and graphene further down. From this the contrast in the phase data from AFM images was interpreted to determine the surface composition at each temperature. [13]

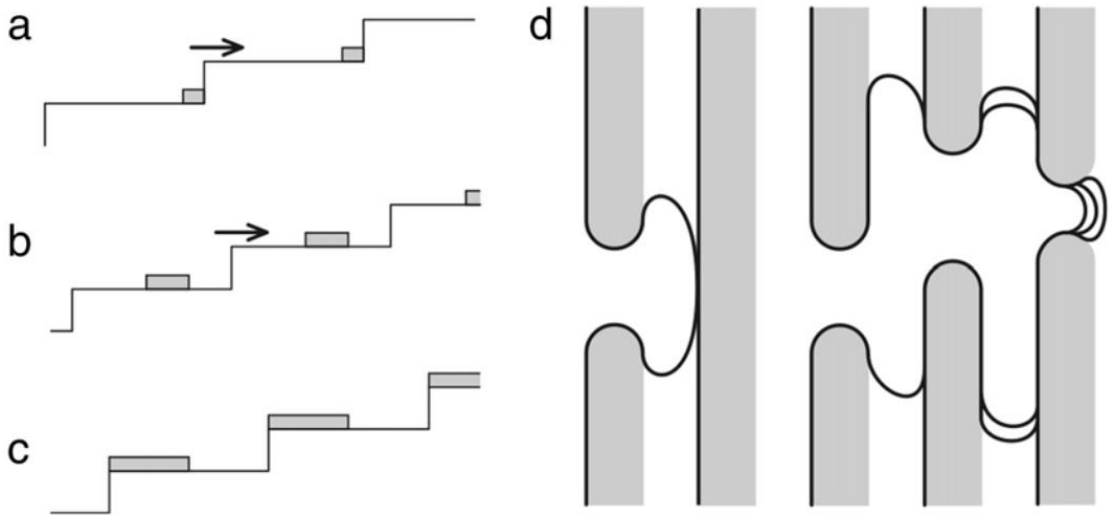

Figure 10. (a) The buffer layer (gray) nucleates at the lower sides of ($\sqrt{3}\times\sqrt{3}$)-reconstructed SiC steps. (b) ($\sqrt{3}\times\sqrt{3}$)-reconstructed SiC steps retract uphill as the buffer layer grows. (c) Eventually a state is reached in which all ($\sqrt{3}\times\sqrt{3}$)-reconstructed SiC steps have been consumed. (d) Pits form when the domains of the buffer layer on each terrace are not continuous and ($\sqrt{3}\times\sqrt{3}$)-reconstructed SiC steps (thick black lines) advance to the next terrace. The image is taken from Ref. [13].

The origin of a pit formation has been tracked to the processes governing the nucleation and growth of the buffer layer, an intermediate layer formed before graphene is grown (at lower temperature) and eventually sandwiched between graphene and the substrate. This buffer layer nucleates on SiC terraces upon consumption of the Si atoms expelled from the SiC(0001) step edges (actually ($\sqrt{3}\times\sqrt{3}$)-reconstructed ones) above 1300 K, leaving regions elongated along the SiC step edges, which are three SiC bilayers-deep, see Figure 10 (a, b). Continued growth of the buffer layer proceeds upon retraction of ($\sqrt{3}\times\sqrt{3}$)-reconstructed SiC steps until these encounter a region covered by a buffer layer uphill of the step (Figure 10c). In practice this leads to stripes of the buffer layer parallel to the initial substrate step edge pattern, except at some locations where the buffer layer stripes are not continuous, where the retraction of the ($\sqrt{3}\times\sqrt{3}$)-reconstructed SiC steps can continue, which leads to the formation of pits (Figure 10d). [13]

At the same time, finger-like structures associated with pits can be found on the surface at 1748 K as illustrated in the Figure 9a. These fingers are formed perpendicular to a step edge and correspond to reconstructed SiC with graphene between them. At higher temperatures as the step edges diminish, the fingers lengthen and eventually become islands after an entire step front has eroded. These islands are found at 1823 K (Figure 9b). Above this temperature the SiC islands shrink further and finally the surface is completely covered by graphene. [13]

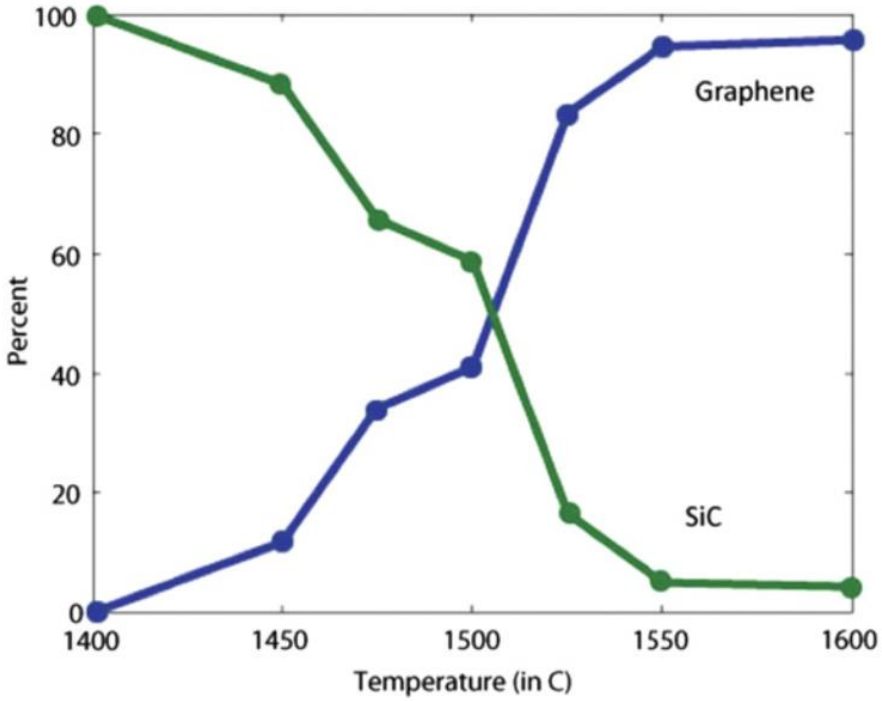

Figure 11. The surface coverage of both graphene (blue) and SiC (green) as a function of annealing temperature. The image is taken from Ref. [13].

The surface coverage of SiC and graphene at different temperatures is shown in the Figure 11. The increase in graphene coverage above 1773 K is accompanied by the reduction of surface features such as pits and fingers, as a graphene layer begins to cover them. At 1873 K graphene completely covers the surface. [13]

The time dependence of the growth was studied by keeping the growth temperature fixed at 1748 K and varying the growth time between 0 and 60 min. AFM images taken at different time intervals show that the surface progresses in almost the same way as when the temperature dependence was studied. Fingers are formed after 2–14 min of growth, which become islands at 16 min. After 60 min the graphene layer is nearly entirely complete. This shows that the growth mechanism for graphene from SiC is the same whether the temperature or heating time is varied. [13]

A better quality of graphene prepared on SiC far from UHV conditions motivated a few studies aiming at unraveling growth processes which could be specific to such conditions. For a SiC(0001) surface almost fully covered by the buffer layer after a 1820 K annealing procedure under Ar atmosphere, further UHV growth yields high quality graphene as obtained by Emtsev et al. [22] who used only non-UHV conditions throughout growth. These findings question a qualitative understanding that the reduction of Si evaporation rate due to the presence of the Ar atmosphere is crucial for slowing down graphene growth close to thermodynamic equilibrium. Instead, the formation of a high quality buffer layer, with the help, for instance, of a high temperature treatment in Ar atmosphere, seems to be the prerequisite for growing high quality graphene. Such a high quality buffer layer should consist of straight triple SiC step edges, separated by large reconstructed (buffer layer) terraces. Such terraces indeed contain about the right amount of carbon necessary for building a full graphene layer on top of the buffer layer in a step flow fashion. The presence

of single SiC steps should be avoided as they lead to the formation of graphene on their side, which, unlike in the case of triple SiC steps, inhibits Si evaporation due to strong C–Si bonds at the SiC–graphene interface. In practice, this leads to the formation of arrow-like growth fronts, as explained in the Figure 12, instead of smooth ones, thanks to which high quality graphene can be obtained. [13]

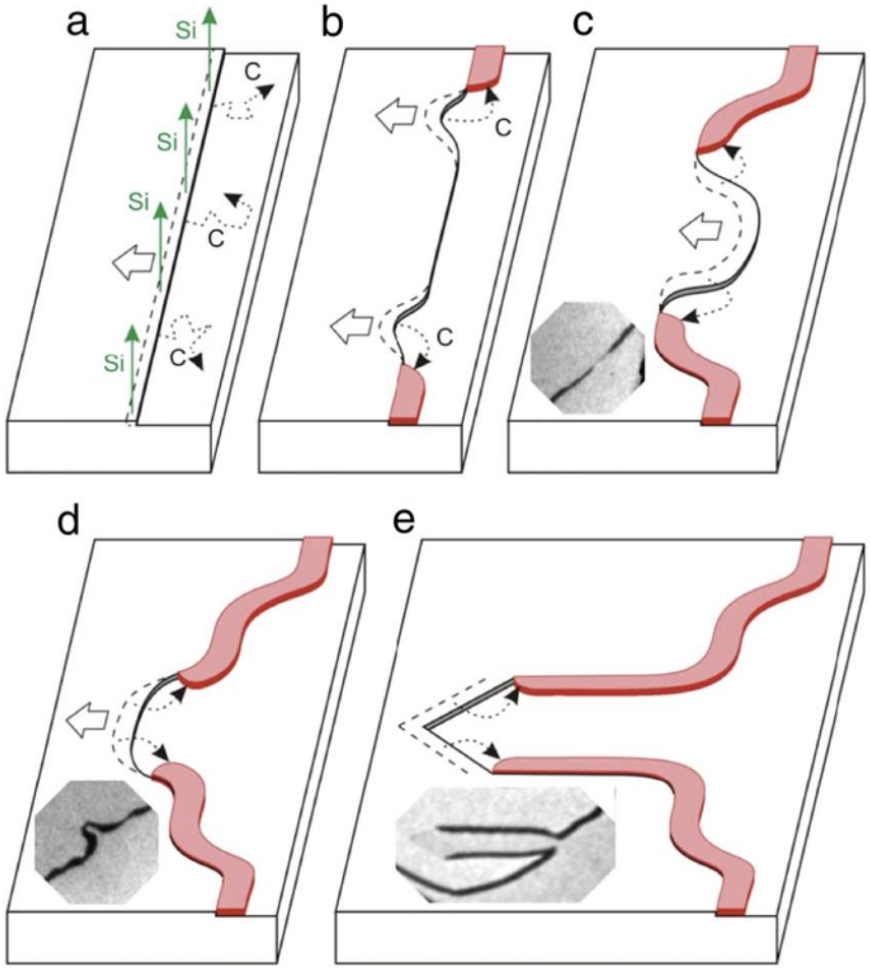

Figure 12. Schematic of the formation of an arrow feature. The insets show static LEEM images of SiC steps at similar stages of evolution. LEEM images are $2\times2\ \mu m^2$ (c, d) and $4\times2\ \mu m^2$ (e). The image is taken from Ref. [13].

In a UHV study, graphene of very high quality has been obtained using evaporation of Si (actually disilane, which readily transforms into Si upon reaching the substrate surface at high temperature, H atoms resulting from its decomposition being efficiently desorbed into vacuum). In this study, different surface transformations of SiC(0001) upon heating could be slowed down considerably, and even reversed by applying an appropriate Si partial pressure. This produced a series of surface transitions in conditions much closer to thermodynamic equilibrium, yielding graphene with a much more uniform number of layers (1–2) and larger-scaled features (few microns) as compared to the situation without Si evaporation (few 100 nm features and 1–4 layers) at the same growth temperature. Further increase in the growth temperature and Si pressure is expected to yield further improved morphology and structure. [13]

3.2.2 Multilayer growth

SiC sublimation often produces multiple graphene layers on top of one another. They can have different properties depending on their interaction with each other and the SiC substrate.

To determine the thickness of graphene layers STM observations of the surface have been used [13]. It was found that the surface roughness can be related to the layer thickness with an exponential relationship. By measuring the surface roughness, steps between upper and lower terraces were identified with a height of 0.4 nm. This height does not correspond to the usual gap between two graphene layers of 0.335 nm. The difference is attributed to the existence of a buffer layer in between the SiC(0001) surface and the graphene layers. This layer has a honeycomb lattice structure with a $\left(6\sqrt{3}\times 6\sqrt{3}\right)R30°$ reconstruction involving the formation of strong C–Si bonds, thus not exhibiting the electronic properties typical of graphene. [13]

As a second graphene layer grows it is calculated from the C density that 3 layers of SiC must be consumed. Because the initial graphene layer continues to cover the surface, it is suggested that the additional layer grows underneath it. Above 1473 K the SiC underneath the buffer layer on the upper terrace decomposes, Si atoms desorb and the liberated C atoms create a graphene layer and a new buffer layer underneath. This bottom-up growth process is depicted in Figure 13. [13]

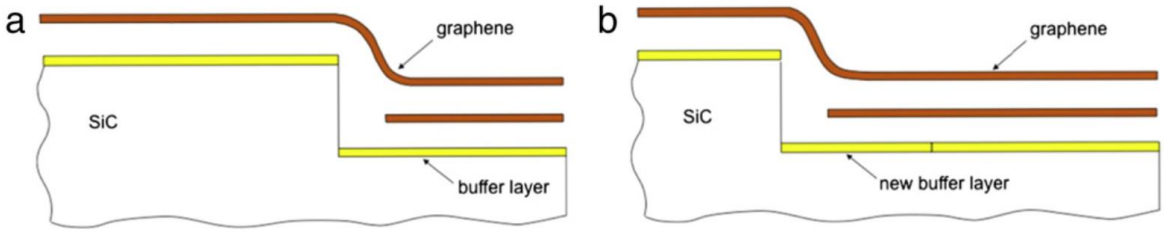

Figure 13. Growth of a second graphene layer at a step edge from the state in (a) to the state in (b). The image is taken from Ref. [13].

Evolution of the growth of graphene multilayers has been observed using low-energy electron microscopy (LEEM) [13]. In order to achieve this, the contrast in the LEEM images was interpreted as the number of graphene layers on the SiC surface. As a check, angle-resolved photoemission spectroscopy (ARPES) was used to determine the populations of the layers from their different photoemission intensities. This was compared with the layer populations found from the LEEM image contrast. As these populations were the same it shows that the LEEM contrast indeed corresponds to the different layer thicknesses. [13]

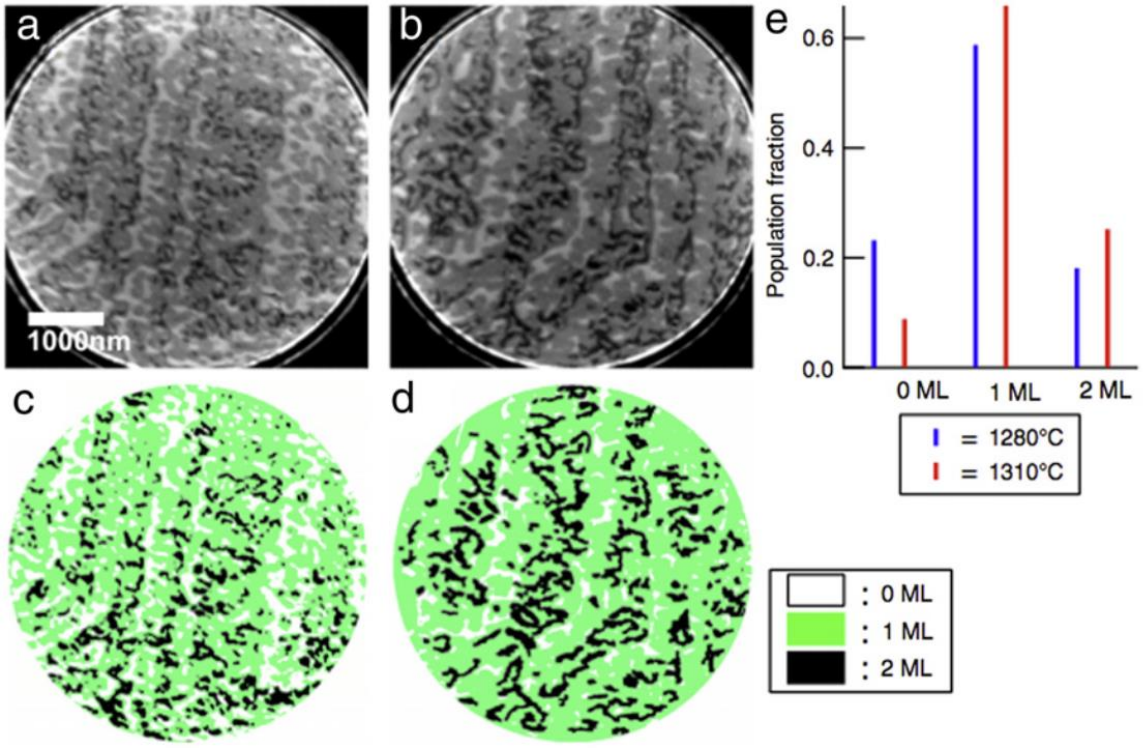

Figure 14. LEEM images of graphene on SiC after heating to (a) 1553 K and (b) 1583 K. (c) and (d) show the regions of different layer thicknesses for (a) and (b) after an object extraction process has been applied. (e) The population fraction of each of these layers at both of the temperatures. The image is taken from Ref. [13].

Using LEEM images of the SiC surface the population fraction of the different graphene layers was determined at 1553 K and 1583 K, see Figure 14e. The light, medium and dark gray regions of the image show graphene-free, single layer and bilayer graphene, respectively, Figure14(a,b). Heating from 1553 to 1583 K causes the graphene-free population to decrease and the single layer and bilayer populations to increase. This shows how multilayer graphene on SiC develops, with new layers growing underneath previous layers, causing the increase in thickness as the temperature is raised. [13]

4 GRAPHENE NANORIBBONS

Graphene nanoribbons (GNRs) are narrow (<50 nm) strips of graphene. The quasi one-dimensional nature of GNRs results in additional advantages over graphene sheets, the more widely known two-dimensional counterpart to GNRs. For example, the high aspect ratio of GNRs significantly lowers the percolation threshold in conductive films and polymer composites, and renders them suitable for spinning fiber from their liquid crystalline alignment. [14]

Graphene nanoribbons have borders which can exhibit edge states and different electronic, chemical and magnetic properties depending on the size and type of the border. The most studied chiral edge configurations (Figure 13), 0° (armchair) and 30° (zigzag), leads to armchair and zigzag nanoribbons (A-GNRs, Z-GNRs). Z-GNRs exhibit edge states, which are not presented in the armchair case. These edge states are presented as a flat band around the Fermi energy level, but extended along the ribbon's edge. It leads to a metallic nanoribbon if the width is large enough (e.g. > 10 nm). Such flat band causes high density of states located at the edges, indicating that they are very reactive sites. Furthermore, Z-GNRs exhibit magnetic properties that are relevant (e.g.) for spintronics. [15]

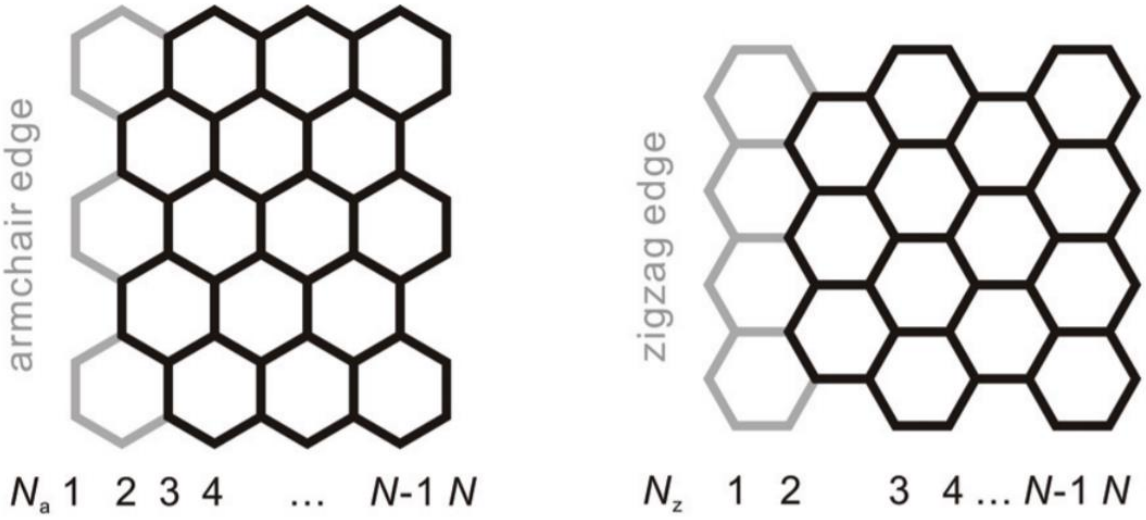

Figure 15. Armchair and zigzag graphene nanoribbon configurations. The image is taken from Ref. [16].

Adopting the standard convention, the width of armchair GNRs is classified by the number of dimer lines (N_a) across the ribbons (Figure 15). Likewise, the one of zigzag GNRs is classified by the number of zigzag chains (N_z) across the nanoribbons (Figure 15). Perpendicularly to the direction of defined width, GNRs repeat their geometric structures, and form one-dimensional periodic structures. Since GNRs are stripes of graphene, edge atoms are not saturated. Active edge states become an important factor to determine the edge structures. For armchair GNRs, there is no any edge reconstruction, and the planar patterns are kept. While for zigzag GNRs, it is unexpectedly found that the zigzag edge is metastable, and reconstructions spontaneously take place at high temperature. [17]

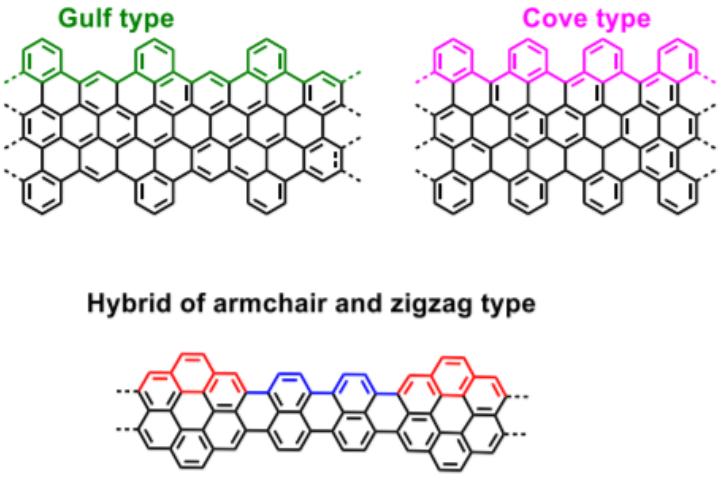

Figure 16. Less common graphene nanoribbon configurations. The image is taken from Ref. [17].

Additionally, the GNRs can be further classified into more types due to the variety of edge structures besides armchair and zigzag, such as “gulf” and “cove” edge structures, and also hybrids of armchair and zigzag edge structures (Figure 16). The GNRs with “gulf” and “cove” edge structures are predicted to show semiconducting behaviors with open bandgaps. For the GNRs with hybrids of armchair and zigzag edges, they display no or limited localized states and also behave as semiconductors with open bandgaps. [17]

5 METHODS OF GRAPHENE NANORIBBONS PREPARATION

There are various methods of graphene nanoribbon preparation. I have conducted a research of literature concerning the topic. The main accent was put on the preparation via SiC sublimation, since it is a feasible way for graphene preparation at the department of microelectronics taking into account available possibilities. Also, attention was paid at the alternative method implying chemical synthesis of graphene nanoribbons from precursors.

5.1 Growth on SiC facets

Growth of graphene nanoribbons on SiC presumes epitaxial graphene growth by SiC sublimation carried out on previously prepared facets. The facets production can be described in the following steps:

1. Covering SiC substrate with lithographically prepared mask having arrays of stripes.
2. Etching.
3. Heating etched substrate to high temperature in ultrahigh vacuum (UHV) or argon atmosphere to induce relaxation of abrupt steps thus forming facets.

The important thing to mention is that the width of facet, prepared by the above described methodology, is dependent on the depth of etching. Thus, the width of graphene nanoribbons forming on those facets can be precisely controlled.

Preparation of facets utilizes common technological processes. Therefore, the technology of graphene growth on SiC was more interesting for taking into consideration. Important parameters and conditions of SiC sublimation conducted by different research groups are specified in the tables below.

Wafer type	n-type 6H-SiC / semi-insulating 4H-SiC (Cree Corp.)	n-type 6H-SiC / semi-insulating 4H-SiC (Cree Corp.)
Wafer orientation	On-axis, Si-face	On-axis, Si-face
Etching	10 lpm of pure hydrogen for 3 min at 1600°C	10 lpm of pure hydrogen for 3 min at 1600°C
Temperature	1320°C	1320°C
Duration	10 min	40 min
Ambience	10^{-8}Torr	10^{-8}Torr
Results	1.9 ML	3.0 ML
Reference	[18]	[18]

Table 2. Summary of SiC sublimation conditions, part I.

Wafer type	n-type 6H-SiC / semi-insulating 4H-SiC (Cree Corp.)	n-type 6H-SiC(0001) with chemical mechanical polishing on the Si face (SiCrystal)
Orientation of wafer	On-axis, Si-face	(0+0.25°), Si-face
Etching	10 lpm of pure hydrogen for 3 min at 1600°C	-
Temperature	1600°C	2000°C
Duration	30 min	-
Ambience	1 atm of Ar (99.999% purity)	1 atm of Ar
Results	the surface is covered with graphene of monolayer thickness	homogeneous single domain graphene layer on most part of the sample
Reference	[18]	[19]

Table 3. Summary of SiC sublimation conditions, part II.

Wafer type	4H- and 6H-SiC(0001) doped with nitrogen (10^{17} to 10^{18} cm^{-3} range)
Orientation of wafer	On-axis
Etching	Hydrogen
Additional wafer preparation	Si deposition
Temperature	1150-1350°C
Duration	-
Ambience	UHV
Results	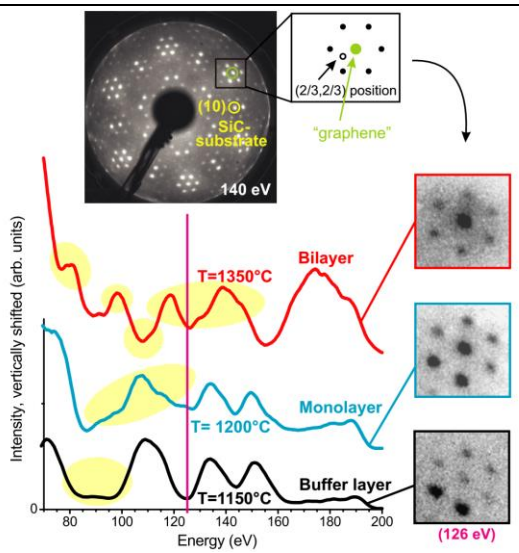
Reference	[20]

Table 4. Summary of SiC sublimation conditions, part III.

Wafer type	N-doped 6H-SiC(0001)
Orientation of wafer	-
Etching	H_2/Ar atmosphere at 1500°C
Additional wafer preparation	annealing at 950°C for 15 min in a Si flux to produce a (3×3) reconstructed surface
Temperature	1300°C
Duration	-
Ambience	UHV
Results	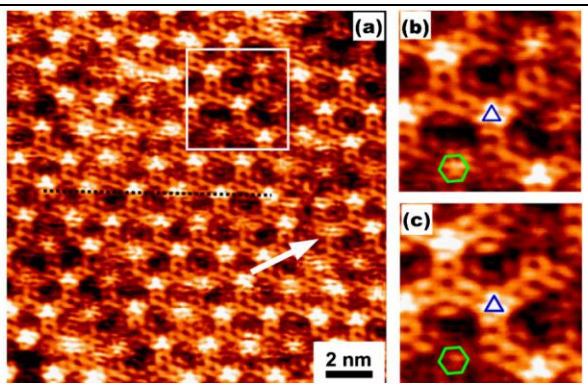
Reference	[21]

Table 5. Summary of SiC sublimation conditions, part IV.

Wafer type	n-type 6H-SiC	semi-insulating 4H–SiC wafer purchased from Cree
Orientation of wafer	3.5° off the (0001) direction	On-axis
Etching	hydrogen	-
Additional wafer preparation	layered 6H-SiC pn junction with a 3-µm thick highly p-doped ($2\times 10^{18} cm^{-3}$of aluminium) layer underneath a 2.9-µm thick slightly n-doped ($1\times10^{15} cm^{-3}$ of nitrogen) layer grown by means of CVD	(0001) target face prepared epiready
Temperature	1650°C	1650°C
Duration	-	120 min
Ambience	Ar flux, 1 atm	1.5 lpm flow of Ar (99.9999% purity), 1 atm
Results	Monolayer graphene for further transistor fabrication	complete graphene film, with regions measuring ~ 30 × 30 µm of unbroken graphene growth
Reference	[22]	[23]

Table 6. Summary of SiC sublimation conditions, part V.

Wafer type	6H-SiC(0001) purchased from SiCrystal AG	4H-SiC (Cree Inc.), 6H-SiC (II-VI Inc.)
Orientation of wafer	On-axis	on-axis (0°±0.5°), C-face
Etching	Hydrogen (grade 5.0, p=1 bar, T=1550°C, t=15 minutes)	Hydrogen
Additional wafer preparation	-	-
Temperature	1650ºC	1550ºC
Duration	-	60 min
Ambience	moderate flow of argon (5.0), 900 mbar	Ar, 100mbar
Results	1.2 ML	epitaxial graphene as incomplete patches across the surface
Reference	[24]	[25]

Table 7. Summary of SiC sublimation conditions, part VI.

Wafer type	4H-SiC (Cree Inc.), 6H-SiC (II-VI Inc.)	4H-SiC (Cree Inc.), 6H-SiC (II-VI Inc.)
Orientation of wafer	on-axis (0°±0.5°), C-face	on-axis (0°±0.5°), Si-face
Etching	Hydrogen	Hydrogen
Additional wafer preparation	-	-
Temperature	1600ºC	1550 and 1600ºC
Duration	60 min	60 min
Ambience	Ar, 100mbar	Ar, 100mbar
Results	Graphene film was continuous	Raman spectroscopy measurements indicated that the films were graphene
Reference	[25]	[25]

Table 8. Summary of SiC sublimation conditions, part VII.

Wafer type	semi-insulating 4H-SiC (Cree, Inc.)	n-doped 4H-SiC
Orientation of wafer	On-axis, Si-face/C-face	On-axis
Etching	a fluorine-based reactive ion etch (RIE) to introduce facets	trench arrays were prepared by first producing a negative ZEP mask by e-beam lithography. The patterned SiC substrate is then reactive ion etched with a SF_6-O_2-Ar plasma to produce up to 30 nm deep trenches depending on etching time
Additional wafer preparation	heating to 1200-1300°C at 10^{-4} Torr to induce relaxation of abrupt steps	The arrays are first annealed at 1100°C for 30 min to stabilize the trench facets
Temperature	1450°C	1525°C
Duration	10 min	1 min
Ambience	Intermediate vacuum (10^{-4} Torr)	confinement controlled sublimation furnace
Results	Presence of graphene at the step edges	Formation of graphene sidewall ribbons
Reference	[26]	[27]

Table 9. Summary of SiC sublimation conditions, part VIII.

The above presented tables with conditions and parameters of SiC sublimation attempts allow for a comparison with the available equipment possibilities in the lab at the department of microelectronics. Characteristics of the equipment are specified further below in the section 5.3. The limitations are given by the properties of the furnace with maximum heating temperature of 1650°C and allowance only for inert gas ambience at the pressure close to atmospheric in the chamber. Therefore considering the above mentioned, I conclude that the most appropriate procedure of SiC sublimation for graphene growth in our conditions was described in the paper [18]. It implies heating of the Si-face 4H-SiC wafers at the temperature of 1600°C for 30 minutes under argon gas atmosphere with the pressure of 1 atm.

5.2 Growth from precursors

Chemical synthesis of graphene nanoribbons presupposes production of GNRs via chemical reactions. The reactions are based on cyclodehydrogenation of precursors, commonly, having benzene ring structures. This approach allows for the direct preparation of GNRs with a well-defined structure and dimensions. Another advantage is relatively easy achievable conditions for the reaction, since it requires much lower (in order of hundreds of

°C) temperatures compared, for example, to epitaxial graphene growth by SiC sublimation. There are several tables below containing summary of the experiments on the above described method conducted by three research groups.

Precursor	5-(6,11-dibromo-1,3,4-triphenyltriphenylen-2-yl)pyrimidine 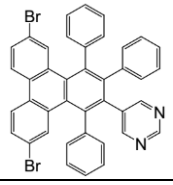
Type of cyclodehydrogenation	Solution-mediated
Reaction chain	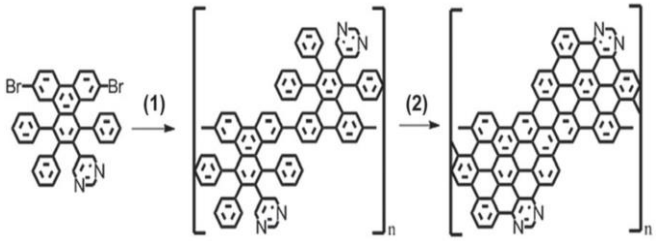 (1) Yamamoto coupling, (2) Scholl reaction
Result	highquality chevron-like 4N-GNRs 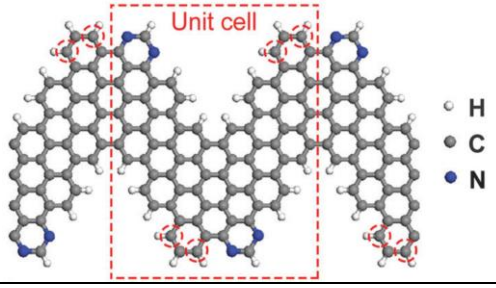
Reference	[28]

Table 10. Chemical synthesis of graphene nanoribbons (GNRs), part I.

Precursor	11,11′- dibromo-5,5′-bischrysene 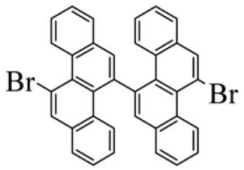
Type of cyclodehydrogenation	Surface-assisted
Reaction chain	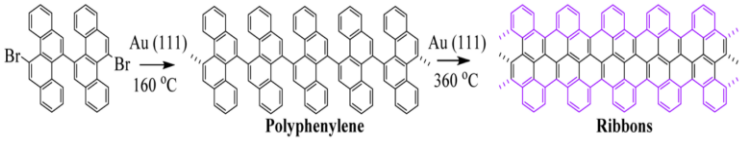
Result	The lengths of the GNRs are up to 20 nm
Reference	[29]

Table 11. Chemical synthesis of graphene nanoribbons (GNRs), part II.

Precursor	1,4,5,8-tetrabromonaphthalene (TBN)
Type of cyclodehydrogenation	Surface-assisted
Reaction chain	dehalogenation of 1,4,5,8-tetrabromonaphthalene (TBN) under ultra-high vacuum (UHV) on Au (111) surface 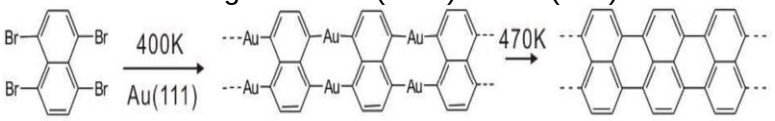
Result	the narrowest n-AGNRs in subfamily of n=3p+2
Reference	[30]

Table 12. Chemical synthesis of graphene nanoribbons (GNRs), part III.

Each process leads to different resulting nanoribbon geometrical structure. This allows for control of the nanoribbon's electrical properties, since its width and chirality affects occurrence of a bandgap, which is required for usage of graphene nanoribbons as semiconductors.

5.3 Available equipment

Conditions and parameters of epitaxial graphene growth by various groups were considered in the section 5.1. In order to choose the most appropriate methodology and to characterize samples of SiC, available equipment will be presented below.

Sublimation of Si from SiC presupposes heating wafers to high temperature. Therefore, a core role of all instrumentation is allotted to a furnace. There is Vecstar THL V1700 tube furnace at the disposal at the department of microelectronics (Figure 17). Its characteristics are listed in the Table 2. The furnace has flanges with through holes at the ends of its tube. Those flanges can be used for the connection of an argon gas cylinder at one end of the tube and a pump on the other.

Figure 17. Vecstar THL V1700 tube furnace.

Maximum temperature	1700ºC
Recommended maximum temperature	1650ºC continuously
Maximum diameter of the ceramic tube	75 mm
Heating tube	Molybdenum disilicide 1800ºC
Length of heated part	300 mm
Regulation controller	Eurotherm 2416
Alarm indicator	CAL
Used thermocouples	Type B
Edges of tube	Flanges for inert atmosphere
Total furnace length	1000 mm
Powering	230 V / 4 kW

Table 13. Vecstar THL V1700 parameters.

Characterization of SiC wafers will be made by means of available in the laboratory of nanolithography atomic force microscope (AFM) based on NTEGRA Prima multifunctional device from NT-MDT (Figure 18).

Figure 18. NTEGRA Prima. The image is taken from Ref. [31].

5.3.1 Setting the furnace

The furnace is set by controller Eurotherm 2416, its front panel is depicted in the Figure 19. The controller allows for fine temperature control over time by means of proportional-integral-derivative (PID) regulation.

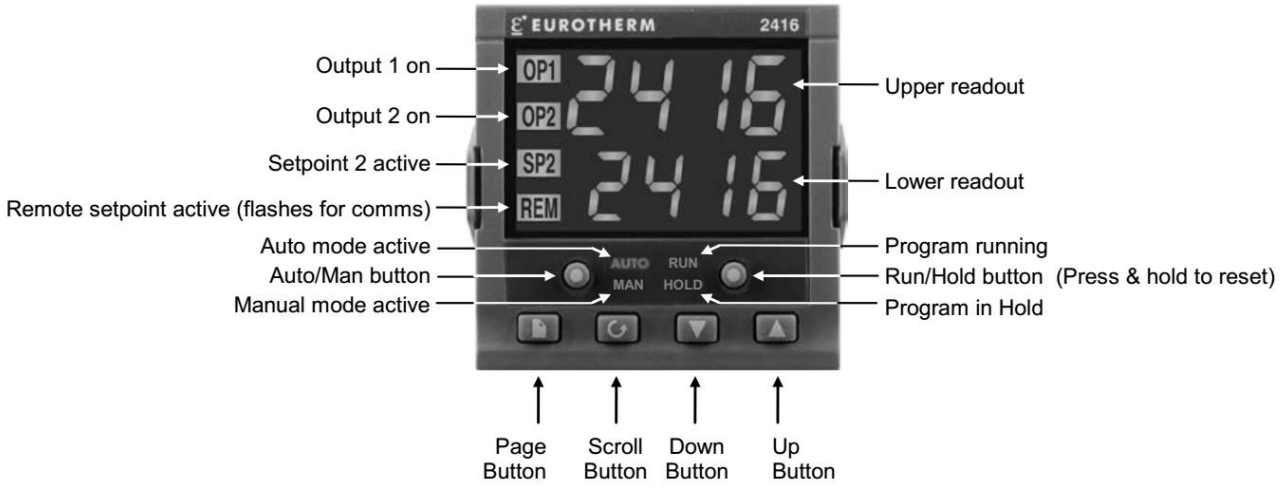

Figure 19. Front panel of the controller Eurotherm 2416. The image is taken from the Eurotherm 2416 user manual.

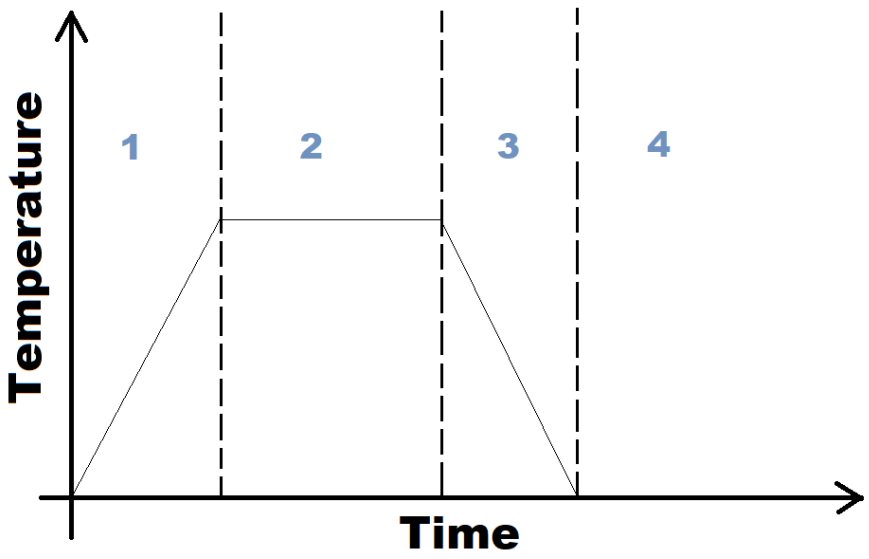

Figure 20. Temperature regime for wafer preparation.

The diagram shown in the Figure 20 represents temperature regime for the epitaxial graphene growth. It was intentionally divided into 4 segments, similar to the way how the controller is programmed. While programming it, you are given the possibility to choose specific parameters of each of 4 segments, such as segment type (ramp, dwell, step), target setpoint temperature, ramp rate (if type ramp is chosen) and duration. A detailed instruction of how to set the depicted heating program is specified in the Appendix.

5.4 Substrate characterization

According to previously studied material, there are basically two possibilities of how graphene commences to form by SiC sublimation: either on step edge terraces, formed because of unintentional miscut of the wafer, or on deliberatly etched facets.

Samples cut from 4H-SiC off-axis wafer from Wolfspeed were obtained for the experiment. The wafer had N-epitaxial layer with the thickness of 52 μm on its top and doping concentration $5 \cdot 10^{14}\mathrm{cm}^{-3}$.

Figure 21 represents AFM analysis of the wafer. As it can be seen, the surface consists of sharp ridges and trenches. Figure 22 shows one of the ridges in greater detail. Its height is approximately 120 nm. One can conclude that possibly those ridges and trenches would facilitate graphene formation under SiC sublimation.

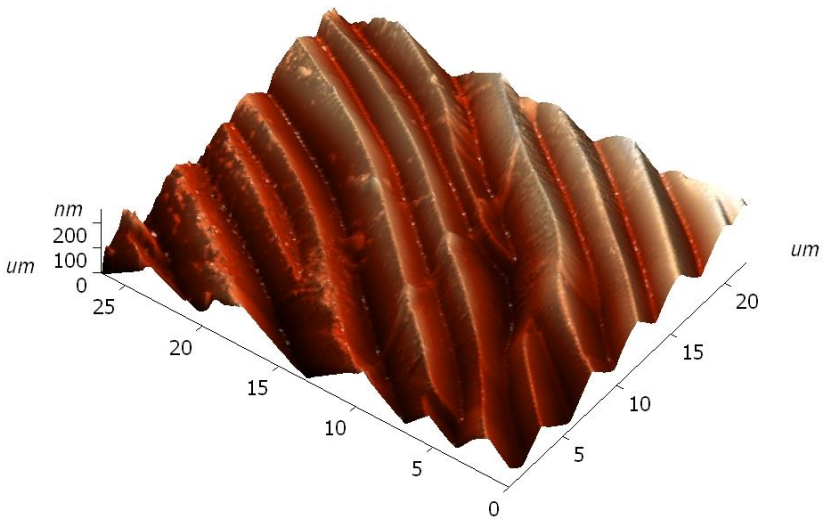

Figure 21. AFM image of the SiC wafer.

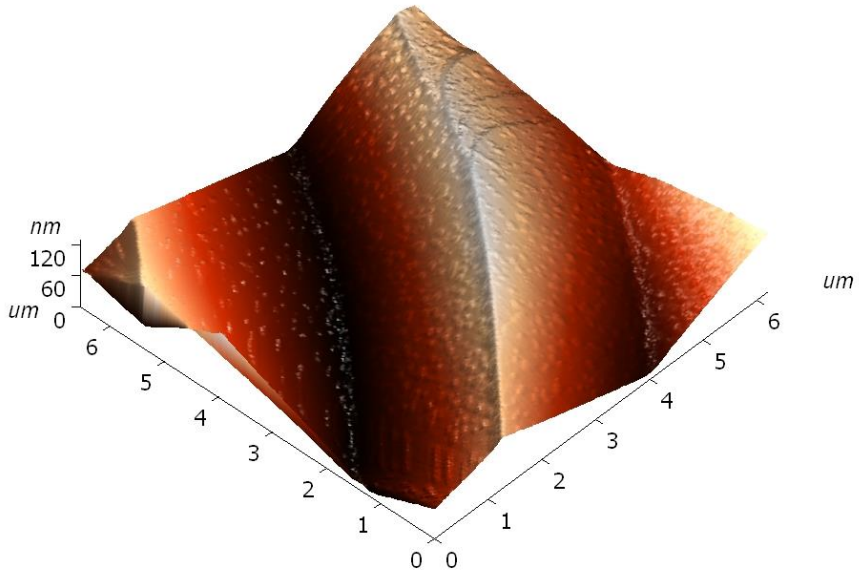

Figure 22. Detailed AFM image of the ridge on SiC wafer surface.

CONCLUSION

The aim of the thesis was to get acquinted with the problematics of graphene as a material, its production techniques and try one of those methods of graphene preparation considering available equipment at the department of microelectronics. In fact, graphene's remarkable properties with brief historical introduction were discussed together with methods of its production, but the initially conceived experimental part failed due to technical problems: the furnace was broken, because the producer did not specify recommended heating ramp rate at the manual (the furnace tube was split due to too high temperature gradient across its length).

However, detailed instruction of the furnace setting was made (section 5.3.1) as well as SiC wafer surface characterization by AFM (section 5.4).

Since the available equipment allowed for only epitaxial graphene growth via SiC sublimation, it was the main focus of the graphene preparation methods research. Conditions and parameters of the experiments conducted by different groups were summarized in the tables in the section 5.1.

As far as the experiment did not take place the attention was paid to a considerably new type of graphene growth method. The method is growth of graphene nanoribbons by chemical approach. Some publications employing chemical synthesis of GNRs were summarized in the tables in the section 5.2.

REFERENCES

[1] N. Z. Haron and S. Hamdioui, "Why is CMOS scaling coming to an END?," *Design and Test Workshop, 2008. IDT 2008. 3rd International,* pp. 98-103, 2008.

[2] I. A. Popov, K. V. Bozhenko and A. I. Boldyrev, "Is graphene aromatic?," *Nano Res.,* vol. 5, no. 2, p. 117–123, 2012.

[3] K. S. Novoselov, A. K. Geim, S. V. Morozov, D. Jiang, Y. Zhang, S. V. Dubonos, I. V. Grigorieva and A. A. Firsov, "Electric Field Effect in Atomically Thin Carbon Films," *Science,* vol. 306, no. 5696, pp. 666-669, 2004.

[4] A. K. Geim and K. S. Novoselov, "The rise of graphene," *Nat. Mater.,* vol. 6, no. 3, pp. 183-191, 2007.

[5] P. R. Wallace, "The Band Theory of Graphite," *Phys. Rev.,* vol. 72, no. 3, p. 258, 1947.

[6] "The Nobel Prize in Physics 2010 - Advanced Information," [Online]. Available: http://www.nobelprize.org/nobel_prizes/physics/laureates/2010/advanced.html.

[7] C. Riedl, Epitaxial graphene on silicon carbide surfaces: growth, characterization, doping and hydrogen intercalation, 2010.

[8] Q. Zheng and J.-K. Kim, in *Graphene for Transparent Conductors*, Springer, 2015, pp. 29-30.

[9] C. Mattevi, H. Kim and M. Chhowalla, "A review of chemical vapour deposition of graphene on copper," *J. Mater. Chem.,* vol. 21, no. 10, pp. 3324-3334, 2011.

[10] J. R. Creighton and P. Ho, "Intodution to Chemical Vapor Deposition (CVD)," in *Chemical Vapor Deposition*, ASM International , 2001.

[11] B. Pollard, "Growing Graphene via Chemical Vapor Deposition," 2011.

[12] W. Norimatsu and M. Kusunoki, "Epitaxial graphene on SiC{0001}: advances and perspectives," *Phys. Chem. Chem. Phys.,* vol. 16, pp. 3501-3511 , 2014.

[13] H. Tetlow, J. Posthuma de Boer, I. J. Ford, D. D. Vvedensky, J. Coraux and L. Kantorovich, "Growth of epitaxial graphene: Theory and experiment," *Phys. Rep.,* vol. 542, no. 3, pp. 195-295, 2014.

[14] A. M. Dimiev and J. M. Tour, "Graphene Nanoribbons: Production and Applications," [Online]. Available: http://www.sigmaaldrich.com/technical-documents/articles/materials-science/graphene-nanoribbons-production-and-applications.html.

[15] A. Barulin, J. Šmarhák and J. Voves, "Simulation of epitaxially grown graphene on step-shaped SiC surface," in *8th Int. Conf. Nanocon 2016* , Brno, 2016.

[16] S. Mikhailov, Physics and Applications of Graphene - Experiments, InTech, 2011.

[17] B. Yang, "Bottom-Up Synthesis of Graphene Nanoribbons and Nanographene Molecules with New Types of Periphery," Mainz, 2015.

[18] Luxmi, N. Srivastava and R. M. Feenstra, "Formation of epitaxial graphene on SiC(0001) using vacuum or argon environments," *J. Vac. Sci. Technol. B,* vol. 28, no. 4, 2010.

[19] C. Virojanadara, M. Syväjarvi, R. Yakimova, L. I. Johansson, A. A. Zakharov and T. Balasubramanian, "Homogeneous large-area graphene layer growth on 6H-SiC(0001)," *Phys. Rev. B,* vol. 78, no. 24, 2008.

[20] C. Riedl, C. Coletti and U. Starke, "Structural and electronic properties of epitaxial graphene on SiC(0 0 0 1): a review of growth, characterization, transfer doping and hydrogen intercalation," *J. Phys. D: Appl. Phys.,* vol. 43, no. 37, 2010.

[21] Y. Qi, S. H. Rhim, G. F. Sun, M. Weinert and L. Li, "Epitaxial Graphene on SiC(0001): More than Just Honeycombs," *Phys. Rev. Lett.,* vol. 105, no. 8, p. 085502, 2010.

[22] S. Hertel , D. Waldmann, J. Jobst, A. Albert, M. Albrecht, S. Reshanov, A. Schöner, M. Krieger and H. B. Weber, "Tailoring the graphene/silicon carbide interface for monolithic wafer-scale electronics," *Nat. Commun,* vol. 3, 2012.

[23] A. J. Strudwick and C. H. Marrows, "Argon annealing procedure for producing an atomically terraced 4H–SiC (0001) substrate and subsequent graphene growth," *J. Mater. Res.,* vol. 28, no. 1, pp. 1-6, 2013.

[24] K. V. Emtsev, A. Bostwick, K. Horn, J. Jobst, G. L. Kellogg, L. Ley, J. L. McChesney, T. Ohta, S. A. Reshanov, J. Röhrl, E. Rotenberg, A. K. Schmid, D. Waldmann, H. B. Weber and T. Seyller, "Towards wafer-size graphene layers by atmospheric pressure graphitization of silicon carbide," *Nat. Mater.,* vol. 8, 2009.

[25] J. L. Tedesco, B. VanMill, R. L. Myers-Ward, J. Culbertson, G. Jernigan, P. Campbell, J. M. McCrate, S. A. Kitt, C. Eddy Jr. and D. K. Gaskill, "Improvement of Morphology and Free Carrier Mobility through Argon-Assisted Growth of Epitaxial Graphene on Silicon Carbide," *ECS Trans.,* vol. 19, no. 5, pp. 137-150, 2009.

[26] M. Sprinkle, M. Ruan, Y. Hu, J. Hankinson, M. Rubio-Roy, B. Zhang, X. Wu, C. Berger and W. A. de Heer, "Scalable templated growth of graphene nanoribbons on SiC," *Nat. Nanotechnol.,* vol. 5, no. 10, pp. 727-731, 2010.

[27] I. Palacio, A. Celis, M. N. Nair, A. Gloter, A. Zobelli, M. Sicot, D. Malterre, M. S. Nevius, W. A. de Heer, C. Berger , E. H. Conrad, A. Taleb-Ibrahimi and A. Tejeda, "Atomic Structure of Epitaxial Graphene Sidewall Nanoribbons: Flat Graphene, Miniribbons, and the Confinement Gap," *Nano Lett.,* vol. 15, no. 1, pp. 182-189, 2015.

[28] T. H. Vo, M. Shekhirev, D. A. Kunkel, F. Orange, M. J.-F. Guinel, A. Enders and A. Sinitskii, "Bottom-up solution synthesis of narrow nitrogen-doped graphene nanoribbons," *Chem. Commun.,* vol. 50, no. 32, pp. 4172-4174, 2014.

[29] J. Liu, B.-W. Li, Y.-Z. Tan, A. Giannakopoulos, C. Sanchez-Sanchez, D. Beljonne, P. Ruffieux, R. Fasel, X. Feng and K. Müllen, "Toward Cove-Edged Low Band Gap Graphene Nanoribbons," *J. Am. Chem. Soc.,* vol. 137, no. 18, pp. 6097-6103, 2015.

[30] H. Zhang, H. Lin, K. Sun, L. Chen, Y. Zagranyarski, N. Aghdassi, S. Duhm, Q. Li, D. Zhong, Y. Li, K. Müllen, H. Fuchs and L. Chi, "On-surface Synthesis of Rylene-type Graphene Nanoribbons," *J. Am. Chem. Soc.,* vol. 137, no. 12, pp. 4022-4025, 2015.

[31] "NT-MDT Spectrum Instruments," [Online]. Available: http://www.ntmdt-si.com/modular-afm/prima.

APPENDIX

Setting of the furnace for the experiment (all pictures are taken from the user manual):

1. Press and simultaneously to get to the home display.
2. Go to “Programmer List” by pressing until following screen appears.

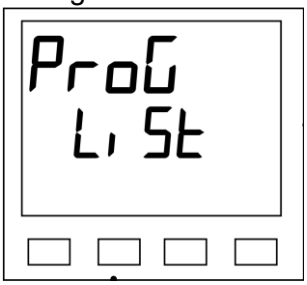

3. Use to scroll between parameters until the following display, further parameters will be related to the first segment.

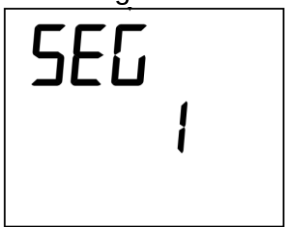

4. Scroll again by pressing until the “type” parameter. Use or to change the first segment’s type to “ramp”, so the following display should occur.

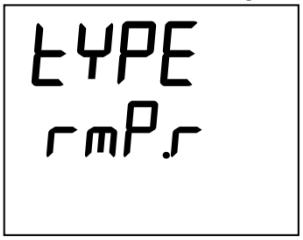

5. Scroll again by pressing until the “target temperature” parameter (following display should appear). Use or to adjust the first segment’s “target temperature” (it is the end temperature for the ramp type segment).

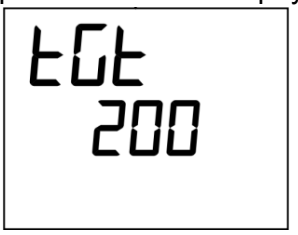

6. Scroll again by pressing until the “ramp rate” parameter (following display should appear). Use or to adjust the first segment’s “ramp rate” (it is how quickly the temperature will change for the ramp type segment).

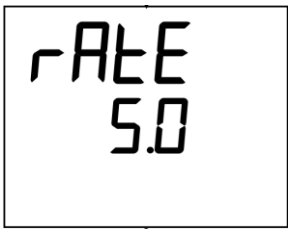

7. Scroll again by pressing ↻ until the following display, further parameters will be related to the second segment.

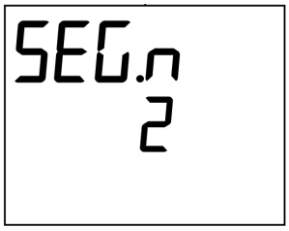

8. Scroll again by pressing ↻ until the “type” parameter. Use ▲ or ▼ to change the second segment’s type to “dwell”, so the following display should occur.

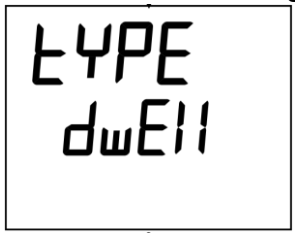

9. Scroll again by pressing ↻ until the “target temperature” parameter (following display should appear). Use ▲ or ▼ to adjust the second segment’s “target temperature”.

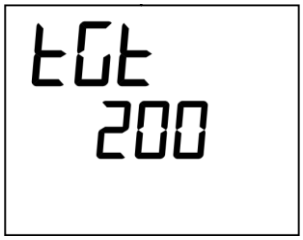

10. Scroll again by pressing ↻ until the “duration” parameter (following display should appear). Use ▲ or ▼ to adjust the second segment’s “duration”.

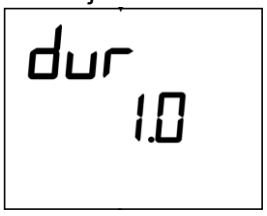

11. Scroll again by pressing ↻ until the following display, repeat steps 4-6 for the third segment.

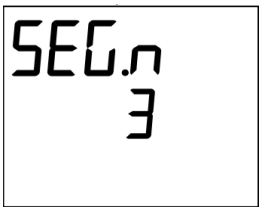

12. Go to “fourth segment’s” parameter “type” by pressing . Change its value to “End”. Following display should occur.

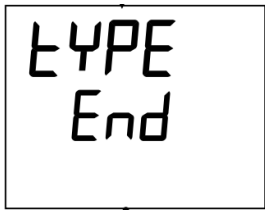

In order to run the program following steps are to be considered (all pictures are taken from the user manual):

1. Press and simultaneously to get to the home display.
2. Go to “Run List” by pressing until following screen appears.

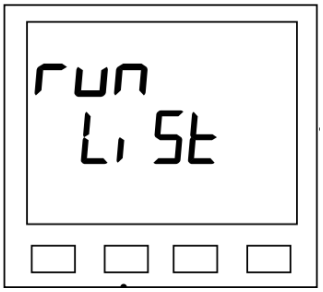

3. Use to scroll until the “status” parameter, use or to change its value to “run”. Following display should occur.